

Local disorder in the oxygen environment around praseodymium in $Y_{1-x}Pr_xBa_2Cu_3O_7$ from x-ray-absorption fine structure

C. H. Booth and F. Bridges

Physics Department, University of California, Santa Cruz, California 95064

J. B. Boyce

Xerox Palo Alto Research Center, Palo Alto, California 94304

T. Claeson

Physics Department, Chalmers University of Technology, S-41296 Gothenburg, Sweden

Z. X. Zhao

National Laboratory for Superconductivity, Institute of Physics, Academia Sinica, Beijing 100080, China

P. Cervantes

Physics Department, University of California, Santa Cruz, California 95064

(Received 14 September 1993)

$PrBa_2Cu_3O_7$ (PBCO) is unique in the $RBa_2Cu_3O_7$ (R =rare earth) series because it is not superconducting. In fact, for $Y_{1-x}Pr_xBa_2Cu_3O_7$, T_c drops monotonically with Pr concentration, with T_c going to zero at $\sim 55\%$ Pr. There have been many studies of this material with the hope that an explanation for the lack of superconductivity in PBCO might help explain why $YBa_2Cu_3O_7$ (YBCO) is superconducting. Explanations center around hole localization, requiring an extra hole on the Y (Pr) site or a localized hole in the O $2p$ shell, at the expense of a mobile hole in the Cu-O planes. To help provide clues that could point to a particular model, and to search for anomalies in the local structure, we present K -edge x-ray absorption fine structure (XAFS) data for various concentrations of Pr in $Y_{1-x}Pr_xBa_2Cu_3O_7$. The character of the Pr K -edge XAFS data indicates that most of the Pr substitutes onto the Y site and is well ordered with respect to the unit cell. These data also show that the amplitude of the first Pr-O peak is greatly reduced when compared to the first Y-O peak in pure YBCO, and decreases with increasing Pr concentration. In contrast, the Y K -edge data for these alloys show little if any change in the oxygen environment, while the Cu K -edge data show a 10% reduction in the first Cu-O peak. Fits to the Pr data suggest that some oxygen atoms about the Pr become disordered and/or distorted; most of the Pr-O nearest-neighbor distances are 2.45 Å, but about 15–40% of them are in a possibly broadened peak at $2.27^{+0.03}_{-0.12}$ Å. The Cu K -edge XAFS data show a slight broadening but no loss of oxygens, which is consistent with a radial distortion of the Pr-O bond. The existence and the size of these two bond lengths is consistent with a mixture of Pr^{3+} and Pr^{4+} bonds, and to a formal valence of $+3.33^{+0.07}_{-0.18}$ for the Pr ion.

I. INTRODUCTION

An interesting property of $YBa_2Cu_3O_7$ (YBCO) is that one may replace yttrium with almost any rare earth and still obtain a high- T_c superconductor,^{1,2} isostructural with YBCO. However, there are two rare earths that do not form a high- T_c superconductor when attempts are made to substitute them onto the Y site: cerium and praseodymium.^{3,4} Attempts to substitute with Ce have not produced the YBCO structure, even in small concentrations. Praseodymium, however, substitutes readily onto the Y site, with T_c dropping monotonically with Pr concentration. Therefore, $PrBa_2Cu_3O_7$ (PBCO) is a unique material in that it has the YBCO structure, with a rare earth instead of Y, yet is not superconducting. In contrast, substitution by Gd, for example, produces essentially no change in T_c or in the crystal structure.⁵

There has been a large effort to explain this reduction in T_c as a new avenue in the search to explain why YBCO is superconducting in the first place. PBCO is interesting in its own right, however, as an insulating layer between layers of YBCO in multilayer films, or as a well matched substrate for epitaxial films of YBCO.

There are many related explanations for the decrease in T_c in $Y_{1-x}Pr_xBa_2Cu_3O_7$ (YBCO:Pr), mostly involving the localization of holes through valence change or magnetic pair breaking mechanisms. The earliest arguments note that Ce, Pr, and Tb are the only rare earths that can exist in either a 3+ or 4+ valent state.⁴ Since Y only exists in a 3+ valent state, one explanation for the decrease in T_c with Pr concentration is that some fraction of the Pr exists in its formal 4+ state, filling a hole state in the Cu-O planes and localizing it onto the Pr site. There is some experimental evidence to support

this view, notably the measured magnetic susceptibility of $2.7\mu_B$ per Pr ion in PBCO,⁶ which may be compared to the Pr^{3+} ion ($3.58\mu_B$) and the Pr^{4+} ion ($2.54\mu_B$). However, this result should be considered in light of some model systems that give moments significantly different than the ionic moments, such as the moment of BaPrO_3 ($0.7\mu_B$),⁷ where Pr^{4+} is presumably the natural state.

Another possible mechanism for suppressing T_c in this material utilizes the fact that, except for Ce, the Pr^{3+} ion is the largest of all the rare-earth 3+ ions. The $4f^2$ electrons are far enough extended to hybridize with the O $2p$ electrons, and thus interfere with the conduction band.⁸ In fact, crystal field measurements can be reconciled with Pr in a completely 3+ state,^{8,9} with broad transitions that can be attributed to hybridization between the Cu $5d$ -O $2p$ states and the Pr $4f$ states.⁹

X-ray absorption near-edge structure (XANES) studies also indicate that Pr is primarily trivalent. Comparisons of the Pr L_{III} edge of PBCO to that for PrO_2 and Pr_2O_3 indicate a valence close to 3+,¹⁰ or slightly above it.^{11,12} The latter studies suggest that a small amount of Pr 4+ is present; Horn *et al.*¹¹ give a mean valence of 3.1+, while Lytle *et al.*¹² find that the valence decreases from 3.45+ for YBCO:Pr 20% to 3.25+ for YBCO:Pr 60% with all of the Pr^{4+} on the Cu(2) site (see Fig. 1 for structural notation). M -edge studies¹³ and electron-energy-loss spectroscopy (EELS) studies¹⁴ also find that the Pr valence is close to 3+. These same studies show that the number of holes in the CuO_2 planes does not change with Pr concentration, while normal-state Hall effect measurements¹⁵ show a decrease in the number of mobile charge carriers with x , indicating that the holes are being localized rather than filled. Photoemission experiments also find that the Pr valence is close to 3+ and that there is significant hybridization of the Pr $4f$ states with other valence states.¹⁶ In addition, thin films of $\text{Y}_{0.5}\text{Tb}_{0.5}\text{Ba}_2\text{Cu}_3\text{O}_7$ have recently been produced, with a T_c of 92 K.¹⁷ Such a high T_c for a 50% terbium sample brings into question the argument that the suppression of T_c arises solely because two valence states can exist.

A theory which combines many of these ideas, proposed by Fehrenbacher and Rice,¹⁸ shows that three electronic configurations are favored: a $\text{Pr}^{3+}(4f^2)$ -O state, a $\text{Pr}^{4+}(4f^1)$ -O state, and a $\text{Pr}^{3+}(4f^2\bar{L})$ -O state, where the $\text{Pr}^{3+}(4f^2\bar{L})$ indicates that the hole does not reside within the praseodymium's electronic structure; rather, the hole is in the ligand. The low-energy ligand hole is obtained via a superposition of O $2p_\pi$ orbitals with f symmetry. The most energetically favorable configuration has Pr^{3+} 60–70% of the time, with the remaining Pr-O bonds split between the other two configurations. They reason that such a mixture would be consistent with all the above measurements, since ionic Pr^{4+} would only exist 15–20% of the time, even though formally the Pr is in a 4+ state 30–40% of the time.

There is also some structural evidence from neutron and x-ray diffraction for a mixed Pr valency. Diffraction results show that PBCO is isostructural with YBCO. The diffraction result for the average Pr-O nearest-neighbor distance of 2.45 Å (Refs. 19–22) is reasonably consistent with Pr^{3+} -O bond lengths in other Pr oxides, such

as in bixbyite Pr_2O_3 , which has a range of Pr-O bond lengths from 2.33 Å to 2.66 Å.²³ It has been noted, however, that both the Cu-O plane separation^{20,22} and the Pr-O(2) and Cu(2)-O(3) bond lengths²² are more consistent with a valence in the range of 3.3–3.4+, as determined by interpolating trends in these bond lengths with rare-earth ionic radius. However, this interpolation argument has at least two possible flaws. First, just because the trend with ionic radius is no longer linear for Pr does not necessarily mean Pr is in a mixed valence state. The Pr^{3+} ion is the largest ion anyone has been able to place between the Cu-O planes in this structure, and so new forces, including more oxygens bonding to the Pr than, say, Y, may be coming into play. In addition, there are several compounds that show a wide range of Pr^{3+} bond lengths, such as bixbyite Pr_2O_3 . Second, if three Pr-O states exist, as suggested by Fehrenbacher and Rice,¹⁸ then one would expect to see two, and perhaps three, different Pr-O bond lengths; Pr^{4+} -O bonds range in length from 2.18 Å in BaPrO_3 to 2.32 Å in PrO_2 . Therefore the three Pr-O states should have bond lengths made up of a long $\text{Pr}^{3+}(4f^2)$ -O, a short $\text{Pr}^{4+}(4f^1)$ -O, and a $\text{Pr}^{3+}(4f^2\bar{L})$ -O (formally, Pr^{4+} -O), whose bond length should be closer to $\text{Pr}^{4+}(4f^1)$ -O. Diffraction would not be sensitive to such a distribution. It will either see the dominant bond length [perhaps the $\text{Pr}^{3+}(4f^2)$ -O], or an average bond length consistent with a mixed valency, depending on the degree of disorder.

Likewise, trends in the local O environment around the Pr with Pr concentration are only obtainable with large Pr concentrations. If trends exist in the concentration region where YBCO:Pr is still superconducting, that is, Pr concentrations $\lesssim 55\%$, diffraction may not see them. Therefore diffraction results do not rule out disorder and/or distortions of the O around the Pr. A distortion in the Pr local structure could indicate the presence of some formal or ionic Pr^{4+} , but other disorder may also exist. For instance, there is experimental evidence from x-ray diffraction to show that the Cu(2)-O(4) distance is anomalously short,²¹ and therefore may impede charge transfer between the planes and the chains. The length of this bond is consistent with the trend with ionic radius of Pr^{3+} ,²² but it is still the shortest Cu(2)-O(4) bond measured in the YBCO-type materials. Any of these results could produce some localization of charge carriers.

Since local distortions and/or disorder in the oxygen environment around praseodymium may indicate the presence of some Pr with a formal valence of 4+, we have conducted x-ray-absorption fine structure (XAFS) experiments on several concentrations of $\text{Y}_{1-x}\text{Pr}_x\text{Ba}_2\text{Cu}_3\text{O}_7$, at the Cu, Y, and Pr K edges ($E_0 \simeq 9$ keV, 17 keV, and 42 keV, respectively). (A preliminary version of this work has recently appeared in the literature.²⁴) XAFS is ideally suited to this problem, because it can give us precise information about the local structure around the absorbing atom, including average bond distances and harmonic broadening factors. In particular, we should be able to determine exactly which site the Pr is occupying and observe changes in the XAFS compared to YBCO. By taking data at three different absorption edges, we can

further constrain our results for the CuO_2 planes and get more information regarding the O(4) site.

In Sec. II we describe some details of the sample preparation and data collection. We explain our data reduction procedures and describe some visible features of the data in Sec. III. Our analysis and fit results are detailed in Sec. IV. We discuss the implications of our results in Sec. V and give a brief conclusion of our findings in Sec. VI.

II. SAMPLES AND DATA COLLECTION

A. XAFS samples

All the samples were prepared by the same procedure as described in Ref. 25. Stoichiometric amounts of CuO , BaCO_3 , Y_2O_3 , and Pr_6O_{11} were mixed, ground, and heated at 920°C in air for 20 h. They were then re-ground, pressed into pellets, calcined at 940°C in an oxygen atmosphere, and slowly cooled at 60°C/h to room temperature. All the $\text{Y}_{1-x}\text{Pr}_x\text{Ba}_2\text{Cu}_3\text{O}_{7-y}$ samples were characterized by x-ray diffraction using $\text{Cu } K\alpha$ radiation. The patterns indicate that all the samples with $x \leq 0.6$ are essentially single phase. The 100% Pr sample may have small amounts of phase impurities, but they are too small to be seen in the XAFS (see Sec. IV). The oxygen content was analyzed by an improved gaseous volumetric technique and found to be within the range of 6.95 ± 0.02 for all samples. In all the compounds T_c was determined by a standard four-probe method. Superconducting phase purity was checked using an ac mutual inductance bridge. Only one step was observed for all superconducting samples. Figure 1 shows T_c as a function of Pr concentration and Table I gives the lattice parameters and the oxygen content measurements for these samples.

XAFS scans were performed on the 0%, 30%, 50%, and 100% Pr samples at about 80 K for the Pr K edge and about 50 K for the Cu and Y K edges. To prepare the samples for these transmission experiments, we re-ground the pellets and sifted the powder through a $30 \mu\text{m}$ filter onto pieces of scotch tape. The tape was then cut and stacked into multiple layers to obtain samples of thickness t , such that $\mu t \simeq 1$ at the absorption edge, where μ is the absorption coefficient. All XAFS experiments were performed at SSRL on beam lines 7-3 and 10-2. Measurements of the incident and transmitted intensities were made with gas-ionization chambers. Si(111) monochromator crystals were used for the Cu and Y K -edge experiments, while Si(400) crystals were required for the Pr K edge.

TABLE I. Sample information: a , b , and c lattice parameters for the $\text{Y}_{1-x}\text{Pr}_x\text{Ba}_2\text{Cu}_3\text{O}_y$ samples.

x	a	b	c	y
0.0	3.821	3.882	11.621	6.96
0.3	3.826	3.894	11.667	6.94
0.5	3.846	3.907	11.691	6.96
1.0	3.902	3.916	11.715	6.98

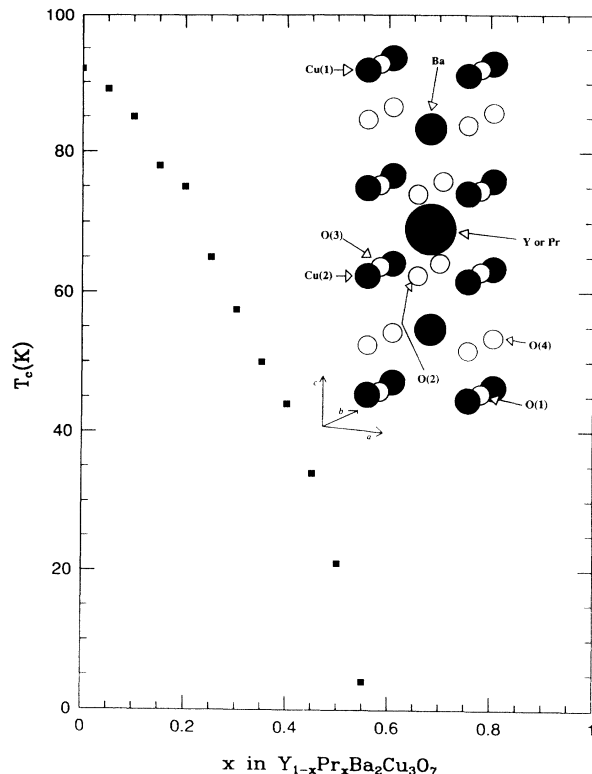


FIG. 1. T_c vs Pr concentration. The inset shows the structure of $\text{YBa}_2\text{Cu}_3\text{O}_7$ with the notation used in this paper.

III. GENERAL FEATURES OF THE DATA

A. Standard reduction and comparison of different absorption edges

Y, Pr, and Cu K edge data for $\chi(k) = (\mu - \mu_0)/\mu_0$ show XAFS oscillations beyond 16 \AA^{-1} for all K edges. Figure 2 shows $k\chi(k)$ for all three K edges for $\text{Y}_{0.5}\text{Pr}_{0.5}\text{Ba}_2\text{Cu}_3\text{O}_7$. The “free atom absorption” μ_0 is determined in the usual way²⁶ by fitting a spline function or a polynomial through the data above the absorption edge. The photoelectron wave vector k is given by $k = \sqrt{(2m_e/\hbar^2)(E - E_0)}$, where E_0 is the K edge threshold energy. This procedure was modified somewhat for the Pr K -edge data, as detailed in Sec. III B.

The most striking difference between the Y and the Pr K -edge XAFS in Fig. 2 is the overall drop in amplitude of the Pr K -edge XAFS, particularly in the low- k part of the spectrum. The amplitudes of the high- k XAFS are similar. The Cu K -edge XAFS are comparable to data we have previously obtained on YBCO.

The Fourier transform (FT) of the data yields peaks in r space corresponding to different radial distances from the excited atom. The peaks in the FT of $k\chi(k)$ are shifted in distance due to phase shifts at the scattering and absorbing atoms, and must be compared to standard compound XAFS to obtain the bond lengths. In the figures showing FT data, the shifted position of the peaks are given by vertical lines. In Figs. 3(a) and 3(b), the

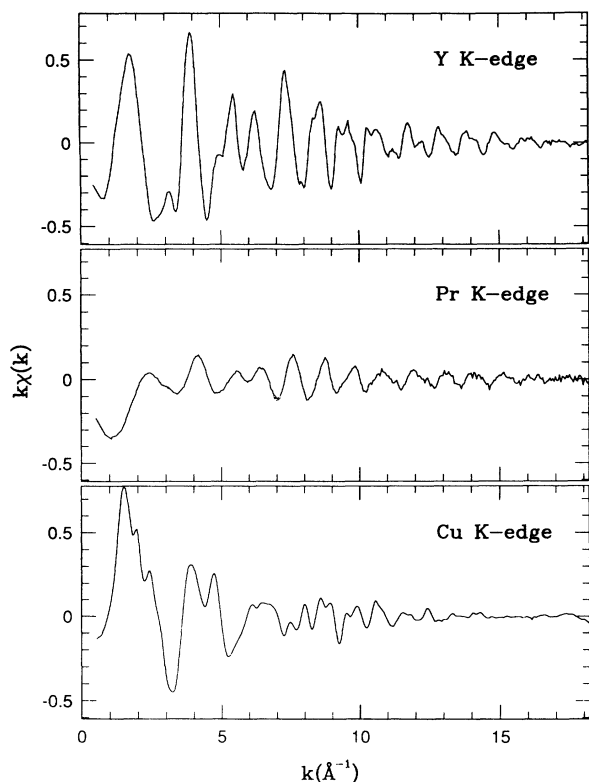


FIG. 2. $k\chi(k)$ for the 50% Pr sample from the Y, Pr, and Cu K edges (at 17080 eV, 41991 eV, and 8979 eV, respectively).

FT of $k\chi(k)$ for data collected on PBCO at the Pr K edge and for CeO_2 at the Ce K edge are compared. FT's for several concentrations of Pr in YBCO:Pr for the Y, Pr, and Cu K edges are presented in Figs. 4, 5, and 6.

By comparing the FT of the XAFS from the various edges, we can quickly ascertain the dominant substitution site for Pr. From the solid line in Fig. 3(a) (PBCO, Pr K edge) and the solid line in Fig. 4 (YBCO, Y K edge) we can see by the location of the first two peaks that the oxygen (first peak) and copper (second peak) environment around Pr in PBCO is very similar to that around Y in YBCO. In contrast, a simulation using FEFF5 (Ref. 27) of the Ba K -edge XAFS in YBCO puts the oxygen and copper peaks at very different positions than observed in the Pr K -edge data. Similarly, the Cu K -edge data for YBCO (Fig. 6) also has a very different environment. This indicates that most of the Pr substitutes at the Y site.

We can also compare the Pr K -edge XAFS for the first Pr-O peak to the Ce K -edge XAFS for the first Ce-O peak in CeO_2 . Both sites should be eight-fold coordinated, and since Ce and Pr are neighbors in the periodic table, their XAFS amplitudes and phases should be comparable. However, the FT of $k\chi(k)$ shows a 60% drop in amplitude in the Pr-O peak in the 100% Pr sample when compared to the Ce-O peak (Fig. 3). In fact, the Pr-O peak amplitude decreases with increasing concentration (Fig. 5). The Pr-Cu peak in PBCO shows little change with concentration, suggesting that the praseodymium is

occupying a well ordered site in the unit cell while the oxygen is not.

Changes in the oxygen environment around the yttrium in the Y K -edge XAFS, if any, are below the resolution of the experiment (Fig. 4). Changes in the further neighbor peaks are only evident in the Y-Ba, Y-Y, Y-Pr regime where the double hump at 3.6 Å becomes less lopsided toward the lower side with increasing Pr concentration. There are no visible changes in the Y-Cu peak.

The Cu K -edge XAFS of PBCO shows a 10% reduction in the oxygen peak amplitude compared to YBCO indicating that some disorder in the oxygen environment exists (Fig. 6). Changes in the Cu-Ba, Cu-Y, Cu-Pr multiplex (between 2.6 Å and 3.4 Å) are complicated, with the large peak at 3.15 Å breaking into two humps at 3.0 Å and 3.3 Å. The peak due to the $[\text{Cu}(1)\text{-Cu}(2)]_c$ axis and

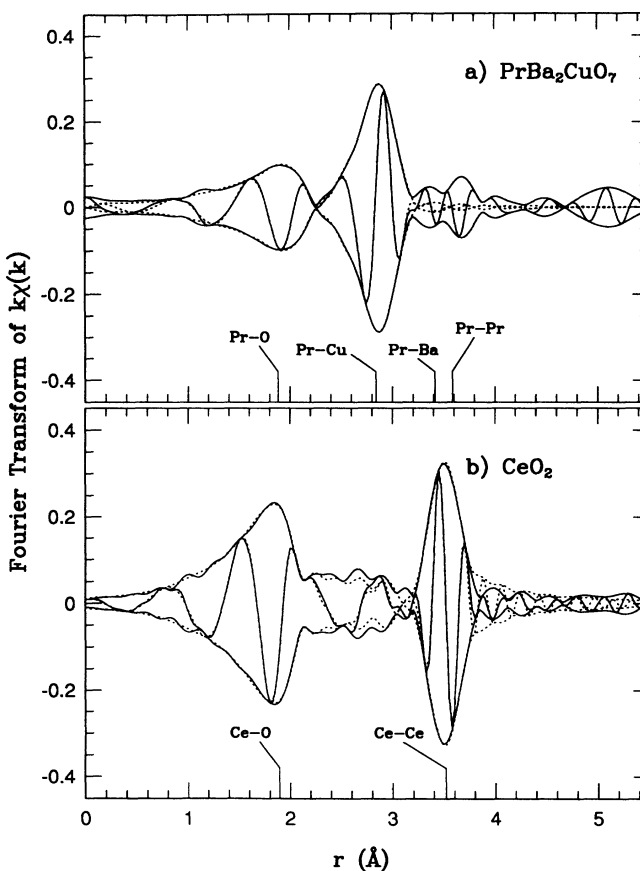


FIG. 3. Fourier transforms of $k\chi(k)$ for (a) $\text{PrBa}_2\text{Cu}_3\text{O}_7$ and (b) CeO_2 , together with fits to the first two major peaks (dotted curve). The outer envelope is the magnitude of the FT, while the modulating curve is the real part. All the fits discussed in the text are of similar quality to the PBCO fit shown here. The first peak in both cases is an eightfold coordinated oxygen peak. Single pair peak positions are approximately given by vertical lines that meet the x axis. These peak positions are shifted from the actual positions by phase shifts at the absorbing and backscattering atoms. Both transforms are from 3.5 to 17.0 Å⁻¹, with a 0.3 Å⁻¹ Gaussian window.

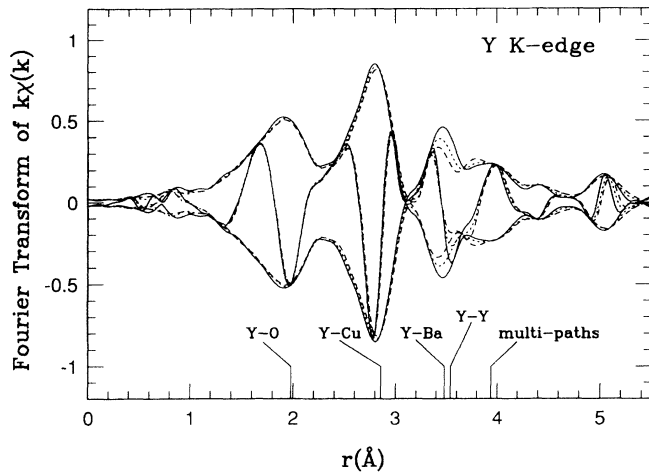


FIG. 4. Fourier transforms of $k\chi(k)$ for Y *K*-edge data for 0% (solid curve), 30% (dotted curve), and 50% (dashed curve) Pr concentrations. The only dramatic changes occur in the Y-Ba, Y-Y, Y-Pr region. These transforms are taken from 3.5 to 15.5 \AA^{-1} , with a 0.1\AA^{-1} Gaussian window.

the *ab* plane Cu-Cu bonds (centered at about 3.65 \AA) decreases monotonically with Pr concentration. This multi-peak includes the forward scattering due to the colinear or nearly colinear oxygens along most of these copper-copper paths. Since the forward scattering amplitude is strongly dependent on small deviations from colinearity,

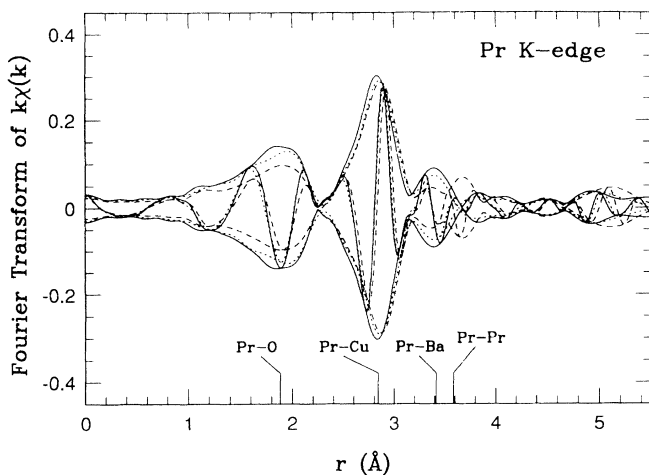


FIG. 5. Fourier transforms of $k\chi(k)$ for Pr *K*-edge data for 30% (solid curve), 50% (dotted curve), and 100% (dashed curve) Pr concentrations. Notice the decrease of the first peak with Pr concentration. This decrease is most likely due to a combination of the relative amplitudes of two Pr-O distances and additional disorder in the shorter bond. The second peak is the Pr-Cu peak. It shows relatively little change with Pr concentration, indicating that the Pr is well ordered with respect to the Cu, and thus to the unit cell. The peaks in the 3–4 \AA range are due to a mix of Pr-Y, Pr-Pr, and Pr-Ba. This region is difficult to fit accurately because the Y and Pr backscattering amplitudes are similar, but π out of phase. The FT ranges are from 3.5 to 17.0 \AA^{-1} , with a 0.3\AA^{-1} Gaussian window.

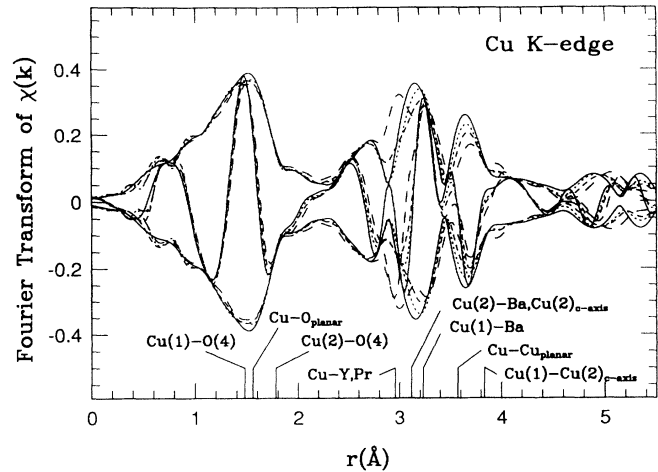


FIG. 6. Fourier transforms of $k\chi(k)$ for Cu *K*-edge data for 0% (solid curve), 30% (dotted curve), 50% (short-dashed curve), and 100% (long-dashed curve) Pr concentrations. The first Cu-O peak decreases with increasing Pr concentration by about 10% in PBCO. The Cu-Y, Cu-Pr, Cu-Ba region also changes dramatically, due to the changing phase shifts between these peaks; see text for further discussion. These transforms are taken from 3.0 to 15.8 \AA^{-1} , with a 0.1\AA^{-1} Gaussian window.

the changes in this peak probably indicate small displacements of the O atoms.

B. Background features in high-energy *K*-edge XAFS

A preliminary FT of the Pr *K*-edge data which uses a simple spline or polynomial for μ_0 indicates an anomalous hump near 1 \AA . By fitting the data above 6 \AA^{-1} to the Pr-O and Pr-Cu peaks, and then subtracting the extrapolated fit from the original data, clear features in $\mu_0(E)$ emerge which cannot be reconciled as an XAFS signal (Fig. 7). The position of the feature roughly 115 eV above the absorption edge is consistent with a multielectron excitation, as estimated from the $Z+1$ model, i.e., with the $N_{IV,V}$ transition of Nd. As pointed out by Holland *et al.*,²⁸ a Ramsauer-Townsend-like effect can also lead to significant structure in the atomic background absorption. Such background features arise when the wavelength of the photoelectron is comparable to the dimension of an “embedded” absorbing atom in a solid and are essentially an XAFS of atomic origin. The effect appears to be larger in atoms of higher atomic number. Calculations by J. Rehr (private communication) show that this structure can occur at energies comparable to those of possible multielectron excitations. The background structure for Pr *K*-edge data is indeed much larger than features we have seen in previous work.²⁹ We have removed the background structure using the iterative procedure discussed in Ref. 29. Similar features were removed from the Ce *K*-edge data for the standard compound CeO₂. Our work on these background features will be the subject of a future paper.

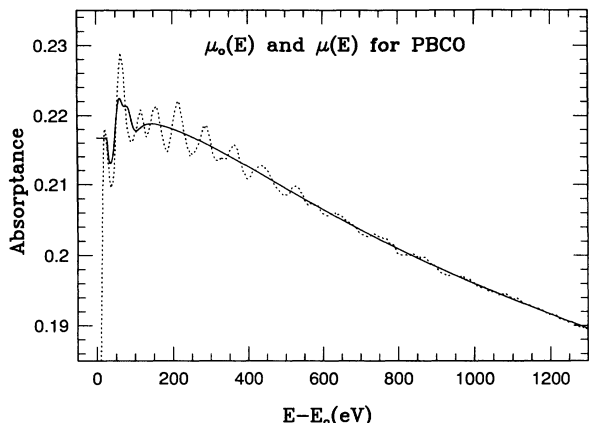


FIG. 7. “Free-atom absorption” μ_0 (solid curve) and total absorption μ (dotted curve) coefficients times sample thickness t , as a function of energy above the K edge. $\mu_0 t$ was determined by an iterative procedure (Ref. 29).

IV. DETAILED ANALYSIS AND FIT RESULTS

A. Fitting procedures and constraints

All fits to the XAFS data are carried out in r space on the FT of $k\chi(k)$. We typically choose an appropriate range in k for the transform, and only fit it in some desired range in r . In the r -space fitting procedure, we vary the XAFS from standard compounds in amplitude, a Debye-Waller-like broadening σ , position, and the K -edge threshold energy E_0 to obtain a good fit. We have developed experimental standards for many pairs of atoms. For pairs which we have no experimental standards, the theoretical standards calculated by FEFF5 (Ref. 27) were used. Fits to the Pr K -edge data used the theoretical standards, while Cu K -edge data were fit with experimental standards. Since we did not obtain standard compounds containing Pr, we evaluated the quality of the theoretical standards for Pr by comparing the Ce-O standard generated by FEFF5 to experimental data obtained from CeO_2 , with good agreement for the Ce-O peak [Fig. 3(b)]. The nonlinear fitting routine minimizes a fit parameter, $C^2 = \sum |\text{FT}(k\chi(k)) - \text{fit}|^2 / |\text{FT}(k\chi(k))|^2$, which is roughly proportional to the statistical χ^2 . Each fit can include some constraints, such as setting the number of neighbors in one peak equal to some fraction of the number of neighbors in another peak. Such constraints are necessary to restrict the number of independent parameters³⁰ and can be used to test a model, or to control correlations between fit parameters. For instance, correlations between amplitude and broadening factors can be controlled by, say, constraining the sum of the number of neighbors for two peaks to be some fixed value. The constraints are generally self-consistent; i.e., various atomic pair distances and number of neighbors are related and must have the same results for measurements at different K edges.

B. Determining substitution site of Pr

A fit to FEFF5 theoretical XAFS standards that includes a mix of Pr at the Y site and at the Ba site indicates that, at most, the Pr exists on the Ba site 8% of the time. This nonzero result could only be obtained if the fit allowed the energy of the Pr K edge (E_0) to be significantly different (10 eV) for Pr in the Y site and Pr in the Ba site. Such a small concentration of Pr at the Ba site in these fits is consistent with all Pr substituting onto the Y site. More information regarding this issue from the other K edges is difficult to obtain, because the backscattering amplitudes of both the Pr ($Z=59$) and Ba ($Z=56$) atoms are very similar.

A similar fit that allows some Pr to reside on the Cu(2) site is not as simple to interpret. For this discussion, we will refer to Pr at the Cu(2) site as $\text{Pr}_{\text{Cu}(2)}$, and Pr at the Y site as Pr_Y . We can obtain a fit to the Pr K -edge data that includes 20% of the Pr residing on the Cu(2) site, with a lengthening of the $\text{Pr}_{\text{Cu}(2)}\text{-O}$ bonds by 0.25 Å and of the $\text{Pr}_{\text{Cu}(2)}\text{-Pr}_Y$ bonds by 0.13 Å. Such a distortion in the oxygen environment is consistent with both the Pr K -edge and the Cu K -edge data. However, a distortion in the $\text{Pr}_{\text{Cu}(2)}\text{-Pr}_Y$ bond should affect how the Pr_Y sits in the unit cell, and should thus be reflected in the $\text{Pr}_Y\text{-Cu}$ bond. This effect should be large even for small ($\sim 20\%$) $\text{Pr}_{\text{Cu}(2)}$ concentrations, because the shift in the $\text{Pr}_{\text{Cu}(2)}\text{-Pr}_Y$ bond length is large enough to cause nearly a complete cancellation of the distorted $\text{Pr}_Y\text{-Cu}$ peaks. The data (Fig. 5) and the fits (see Sec. IVD) show very little change in the Pr-Cu peak. Therefore, these data are not consistent with Pr at the Cu(2) site within the amplitude limits of XAFS spectra ($\sim 10\%$), for all Pr concentrations measured.

C. Y K -edge fits

Fits to the Y K edge data were performed, without any constraints, on the 0%, 30%, and 50% Pr samples. Results for the oxygen and copper peaks are given in Table II. Further peaks, such as the Y-Ba, Y-Pr, and Y-Y peaks, were fit but are not reported, because they are all at similar distances, and the Y-Ba, Y-Pr peaks are almost exactly out of phase with the Y-Y peak. This situation allows changes in amplitude to be mimicked by changes in position, and thus does not give reliable results.

The number of oxygen neighbors shown in Table II changes very little with concentration (about 5% up to 50% Pr), while the copper peak shows a slight increase. Such small changes are not within the resolution of this experiment, and the data are therefore consistent with no change in the number of O atoms surrounding Y. The Y-O distance remains constant. The Y-Cu distance does increase monotonically with Pr concentration, as one would expect from the diffraction results (Table I).

TABLE II. Y *K*-edge fit results. These fits include further peaks than the Y-Cu peak, but these peaks are plagued by an interference effect when Pr is present (see Sec. IV D). Y-Cu amplitudes are consistently larger than those calculated by FEFF5 by nearly 25%. Since we do not have data for a similar standard pair, we have normalized the Y-Cu number of neighbors to the YBCO result. The number of Y-O neighbors is not normalized. The fits are from 1.0 to 3.1 Å in *R*, and from 3.5 to 17 Å⁻¹ in the wave vector *k*. Each bond is expected to be comprised of eight neighbors. The errors are ±0.01 Å in *R*, and ±10% in both σ and number of neighbors for all XAFS fits reported in this work, unless otherwise noted.

<i>x</i>	Y-O			Y-Cu		
	<i>R</i> (Å)	Neighbors	σ (Å)	<i>R</i> (Å)	Neighbors	σ (Å)
0.0	2.41	7.3	0.058	3.21	8.0	0.058
0.3	2.41	7.1	0.056	3.22	8.6	0.060
0.5	2.41	6.9	0.057	3.23	8.6	0.060

D. Pr *K*-edge fits to a variety of models

Fits to the Pr *K*-edge XAFS spectra were performed with and without a variety of constraining models and initial conditions. Each model has an associated C^2 value for its fit, which should give the reader a feel for the range of models that may give plausible results. Table III gives fits to the 100% Pr sample with a variety of constraints imposed on the fits that simulate different models. None of the models constrain the Pr-Cu peak, and none of the fits to these models show any significant differences in this peak.

Model 1 assumes a single Pr-O bond, with no constraints, and gives a good quality of fit. This fit shows an oxygen deficiency around Pr, with only 4.8 of the expected 8 oxygens. Since this result is inconsistent with the fit results of the Y *K* edge (Sec. IV C), the Cu *K* edge (Sec. IV E), and the volumetric measurements of the oxygen concentration in these samples (Table I), we constrained the next fit to give eight oxygens. Model 2, which has one Pr-O distance and does not allow for an oxygen deficiency, yields a poor fit with a substantially larger σ and an increase in the goodness-of-fit parameter (C^2) by more than an order of magnitude. It is therefore highly unlikely that simple harmonic disorder of the

Pr-O bond can explain the reduction in the Pr-O peak in the FT of $k\chi(k)$.

Next we considered several models that allow the first peak to be composed of two different Pr-O harmonic distributions. Since for *K*-edge data any shift due to differences in valence should be small, all of these models constrain any E_0 shifts in the Pr-O bonds to be the same. Model 3 allows for a double Pr-O bond, with no further constraints. This fit has the best C^2 of any of the models. It indicates a total number of oxygens which is still low (5.7). However, a fit to model 4, which constrains the total number of nearest-neighbor oxygens to sum to 8, gives a C^2 which is only 30% higher.

Two other models were tested to see if the fits in models 3 and 4 can be distinguished from similar models. All these fits have a good quality of fit parameter, but shift certain parameters outside a reasonable range. A fit which constrains the length of the two bonds to be equal and the total number of oxygens to be 8 (model 5), but allows for different σ 's gives a very large σ of 0.287 Å for the short Pr-O bond, with 3.5 O neighbors (roughly 36% of the O). However, a peak this broad has a tiny XAFS amplitude, and therefore this fit is essentially the same as the single Pr-O peak fit in model 1. Consequently we do not consider this possibility further. Constraining the

TABLE III. Fit results on PrBa₂Cu₃O₇ to a variety of models. Fitting procedures are detailed in the text. C^2 is the fitting parameter, and is approximately proportional to the statistical χ^2 , as described in the text. The *r*-space fits are from 1.0 to 3.0 Å in *R*, and the FT from 3.5 to 17.0 Å⁻¹ in the wave vector *k*. The number of Pr-O neighbors is normalized to the CeO₂ result. No normalization has been applied to the Pr-Cu peak. Model 1 only allows for one Pr-O distance, with no constraints on the fit parameters. Model 2 also only allows for a single Pr-O bond, but constrains the amplitude to be 8, as is expected from the known crystal structure. Model 3 allows for two Pr-O bonds (Pr-O_{short} and Pr-O_{long}, as do all the subsequent models) with no further constraints. Model 4 constrains the total number of Pr-O bonds to 8. Model 5 constrains the number of Pr-O bonds to 8 and holds their bond lengths equal. Model 6 constrains the total number of Pr-O bonds to 8 and holds their broadening factors (σ) equal.

Model	Pr-O _{short}			Pr-O _{long}			Pr-Cu			C^2
	<i>R</i> (Å)	Neighbors	σ (Å)	<i>R</i> (Å)	Neighbors	σ (Å)	<i>R</i> (Å)	Neighbors	σ (Å)	
1				2.46	4.8	0.066	3.27	7.8	0.049	0.148
2				2.47	8.0	0.116	3.27	7.6	0.047	1.513
3	2.30	1.0	0.135	2.46	4.7	0.063	3.27	7.9	0.048	0.132
4	2.27	2.9	0.168	2.45	5.1	0.067	3.27	7.7	0.048	0.174
5	2.46	3.5	0.287	2.46	4.5	0.064	3.27	7.8	0.048	0.160
6	2.15	1.2	0.084	2.44	6.8	0.084	3.27	7.7	0.048	0.300

TABLE IV. Pr K -edge fit results to $Y_{1-x}Pr_xBa_2Cu_3O_7$ as in model 4 in Table III.

x	R (Å)	Pr-O _{short}		R (Å)	Pr-O _{long}		R (Å)	Pr-Cu	
		Neighbors	σ (Å)		Neighbors	σ (Å)		Neighbors	σ (Å)
0.3	2.25	1.7	0.128	2.43	6.3	0.056	3.25	7.5	0.046
0.5	2.29	2.7	0.115	2.43	5.3	0.053	3.25	7.4	0.047
1.0	2.27	2.9	0.168	2.45	5.1	0.067	3.27	7.7	0.048

σ 's to be equal (rather than the bond lengths), with eight total oxygen neighbors (model 6) gives a fit with a short Pr-O bond length of 2.15 Å and an increase in C^2 by less than a factor of 2 over model 4. In this fit, only 15% of the Pr-O bonds are short. Such a short bond length is not unreasonable, given that the short Pr-O bond in $BaPrO_3$ is 2.18 Å,²³ although Pr is only sixfold coordinated with respect to oxygen in that compound. Models 3, 4, and 6 all indicate that the radial distribution of Pr-O bond lengths is not a symmetric distribution; the major weight is near 2.45 Å but there is clearly some weight in a broad peak centered near $2.27^{+0.03}_{-0.12}$ Å.

Fits that allow for three Pr-O distributions (as suggested by Ref. 18) are not conclusive, because the number of parameters required for such a fit exceeds the maximum number of parameters allowed by our fitting range.³⁰ However, the two peak fits described above giving large σ 's for the shorter Pr-O distribution may mimic a situation with three distances.

The fits that allow for two Pr-O distributions give the most consistent results. These fits (models 3–6) suggest that 15–40% of the nearest-neighbor Pr-O bonds are either disordered and/or shifted ($\simeq 0.18$ Å) compared to a more populated, ordered site.

Table IV summarizes the results of a two-peak fit with the constraint that there be eight oxygens in the first peak for all measured Pr concentrations. Debye-Waller factors for the disordered site increase linearly with Pr concentration, and are as much as 150% higher than for the “normal” site in PBCO. The fits show no appreciable change in the Cu environment around praseodymium with concentration, apart from the expected lengthening of the Pr-Cu bond due to the slight expansion of the lattice (Table I). The number of copper neighbors around

the praseodymium remains the same for the 100% Pr sample compared to the other Pr concentration samples. Therefore, we can conclude that the effect of the small fraction of other phases in the PBCO sample²⁵ on the XAFS is below the resolution of the experiment.

E. Cu K -edge fits

Cu K -edge fits to the 0% and 100% Pr samples were also carried out. Fits to partial concentrations of Pr are difficult to obtain because of the known distortions caused by the two sublattices. Several constraints were placed on the fits to maintain certain symmetries in the system. For instance, the Cu(1)-O(4) distance plus the Cu(2)-O(4) distance is constrained to equal the Cu(1)-Cu(2) distance obtained from diffraction.²¹ The Ba position is constrained to be in the center of the ab plane of the unit cell, while the Y or Pr position is constrained to be in the middle of all planes in the unit cell, consistent with the Cu(2)-Y and the Cu(2)-Cu(2) (c -axis) bond lengths. Other constraints on the number of neighbors have been imposed to maintain the number of atoms at certain sites while still allowing for overall shifts in amplitude. The proximity of the Cu(1)-O(1), Cu(2)-O(2), and Cu(2)-O(3) peaks makes an accurate determination of their relative amplitudes difficult. Consequently, measurements of changes in their relative amplitudes are beyond the resolution of our fits. We have treated the Cu(1)-O(1), Cu(2)-O(2), and the Cu(2)-O(3) as one peak (the Cu-O_{planar} peak), and constrained the relative amplitudes of this peak to the Cu(1)-O(4) and the Cu(2)-O(4) peaks.

The fits to the Cu K -edge data are summarized in Ta-

TABLE V. Cu K -edge fit results to $YBa_2Cu_3O_7$ (YBCO) and $PrBa_2Cu_3O_7$ (PBCO). The “pseudo-YBCO” is calculated from the lattice parameters of PBCO (Ref. 21) and the relative atomic positions in YBCO (Ref. 31). The last column shows the differences between the XAFS results and the diffraction results for PBCO. The samples used in the diffraction measurements for PBCO had a mean oxygen content of $\simeq 6.77$. The PBCO XAFS results agree with the diffraction results, within calculated errors, except for the Cu(1)-O(4) and the Cu(2)-O(4) bond lengths, as discussed in Sec. V. The calculated errors are the same as discussed in Table II except for the Cu-Ba, Pr neighbors in PBCO (± 1.5), and the positions of the Cu-Ba, Pr, and Y peaks for both PBCO (± 0.03 Å) and YBCO (± 0.02 Å).

Bond	Expected Neighbors	PBCO XAFS			YBCO XAFS			Pseudo-YBCO R (Å)	PBCO diffraction ^a R (Å)	XAFS diffraction R (Å)
		R (Å)	Neighbors	σ (Å)	R (Å)	Neighbors	σ (Å)			
Cu(1)-O(4)	2	1.88	2.4	0.082	1.85	2.3	0.069	1.856	1.849	+0.031
Cu-O _{planar}	10	1.98	11.8	0.082	1.94	11.7	0.069	1.965	1.965	+0.015
Cu(2)-O(4)	2	2.22	2.4	0.056	2.27	2.3	0.110	2.311	2.254	-0.032
Cu(2)-Ba	8	3.36	9.5	0.056	3.37	7.6	0.035	3.408	3.388	-0.018
Cu(1)-Ba	8	3.47	9.5	0.056	3.49	7.6	0.035	3.499	3.482	-0.012
Cu(2)-Y,Pr	8	3.23	9.5	0.051	3.21	7.6	0.051	3.232	3.265	-0.025

^aReference 21.

ble V. Fit parameters for YBCO are typical of fits we have obtained in previous work. There are several differences between the YBCO and the PBCO results. Bond length changes are, of course, expected, and will be dealt with in some detail in the next section. The number of neighbor values is 15% different for the combined Ba and Pr peaks compared to YBCO, which is usually considered to be outside the expected error (10%) for XAFS amplitudes. However, the amplitude of this combined peak is very sensitive to the individual positions of the Ba and the Pr, as well as to the position of the $\text{Cu}(2)\text{-Cu}(2)_{c\text{ axis}}$ peak, and is therefore not very reliable. The broadening factors are slightly larger for the planar oxygens and the $\text{Cu}(1)\text{-O}(4)$ bond in PBCO, as are the σ 's for the Ba and Pr peaks. The $\text{Cu}(2)\text{-O}(4)$ bond in PBCO is much narrower than in the YBCO. Again, the σ 's for the Ba and Pr peaks suffer from the same problems as their amplitudes, but the change in σ for the oxygen peaks is probably real.

V. DISCUSSION

A. Consistency between various *K*-edge data

Since each absorption edge gives us information about the oxygen environment within YBCO:Pr, we can constrain our results to give a consistent picture. Y *K*-edge data show little if any change in the structure of YBCO:Pr up to 50% Pr, except (possibly) in the expected lengthening of the Y-Cu bond. Even this expansion of the Y-Cu distance is at the edge of the accuracy of this experiment. These data therefore show that up to 50% Pr, the oxygen and copper environment around yttrium in YBCO:Pr is essentially the same as in pure YBCO. More specifically, there is little evidence of a loss of oxygens or of disorder in the oxygen or copper environment.

The Pr *K*-edge data and fit results indicate that either there are missing oxygens in the Cu-O planes or that there is a large amount of disorder and/or distortion in these planes. The former is inconsistent both with the measured oxygen content and with the number of neighbors for the Cu-O and the Y-O peaks in the XAFS data, and is therefore ruled out. The data are best fit by two Pr-O distributions, separated in pure PBCO by about 0.18 Å, with one distribution less populated and more disordered than the other.

The Cu *K*-edge data are more complicated because of the two copper sites. Nevertheless, the oxygen environment as seen from the coppers should be consistent with (and therefore can help constrain) the Pr *K*-edge results. The fit results to the oxygen peaks show essentially no change in the number of nearest neighbors, but indicate a broadening in the $\text{Cu-O}_{\text{planar}}$ peak consistent with the 10% decrease in the peak height. If the Pr-O distortion is completely radial, then a shortening of 0.18 Å would correspond to only a 0.04 Å lengthening of $\sim 30\%$ of the $\text{Cu}(2)\text{-O}(2,3)$ bonds, which is not resolvable in the fits. However, such a distortion will contribute to a broadening of the $\text{Cu-O}_{\text{planar}}$ peak, and therefore the measured

broadening is consistent with the proposed radial distortion in the Pr-O bond. The small change in the number of Y-O neighbors (which can also be modeled as a slight increase in σ) is also consistent with a radial distortion in the Pr-O bonds.

B. The question of valence

The fit results to the first oxygen peak from all three edges are consistent with a distortion of the Pr-O bond in the radial direction of approximately 0.18 Å. This distortion may be due simply to a hybridization of the O *2p* and Pr *4f* electrons. However, the magnitude of the shift is very consistent with some Pr^{4+} ; the best fit gives a $\text{Pr-O}_{\text{short}}$ bond length (2.27 Å) which is close to the nearest-neighbor bond length in eightfold coordinated PrO_2 . By constraining the broadening factors, we can obtain a much shorter bond length (2.15 Å) which is more consistent with sixfold coordinated BaPrO_3 . The comparison to the eightfold coordinated PrO_2 makes the most sense, since Pr in PBCO is eightfold coordinated, although it is possible that not all the oxygens participate in Pr-O bonds.

If we assign all of the short Pr-O bond lengths to the formal Pr^{4+} state, our fit results indicate that the Pr is in that state 15–40% of the time, corresponding to a formal valence of $+3.33_{-0.18}^{+0.07}$. Such an assignment is reasonable for the shortest measured Pr-O bond length, but if the bond length is closer to ~ 2.3 Å, then some could still include Pr^{3+} , as in bixbyite Pr_2O_3 . Therefore, the upper limit on the valence range may be too high. Likewise, the lower limit was obtained by forcing the broadening factor of the short bond to be much lower than in the best fit, which may not be reasonable.

The possible disorder in the shorter Pr-O bond could cause localization of charge carriers, and could be a by-product of a *4f-2p* hybridization. On the other hand, since the disorder is greatest for the PBCO sample, the disorder could be due to the less common $\text{Pr}^{4+}\text{-Pr}^{4+}$ combination, which will probably have different Pr-O bond lengths than either the $\text{Pr}^{3+}\text{-Pr}^{3+}$ or the $\text{Pr}^{3+}\text{-Pr}^{4+}$ combinations.

Our measured dominant Pr-O distance of 2.45 ± 0.01 Å is in excellent agreement with diffraction results^{19–22} that give a mean Pr-O distance of 2.4539 ± 0.0038 Å. We see no evidence of a longer distance ($\simeq 2.5$ Å) as suggested by the Pr-O bond length trend with ionic radius.²² Fits that include such a peak invariably shift the peak back to the values we report. Therefore, we must conclude that the discrepancy of this bond length with ionic radius is not directly due to a mixed valency. Indeed, given the existence of a short Pr-O bond, the long Pr-O bond seems to be entirely $\text{Pr}^{3+}(4f^2)\text{-O}$.

The range for the valence is in approximate agreement with the electronic studies mentioned in Sec. I that give the valence of Pr to be close to 3+. However our results clearly suggest a higher formal valence than 3.0, as was found in Pr *L*-edge studies of Horn *et al.*¹¹ (3.1+ for PBCO) and Lytle *et al.*¹² (3.45+ for 20% Pr and 3.25+ for 60% Pr). In addition, our structural results show that

the number of short Pr-O bonds, that is, formal Pr^{4+} , increases with increasing Pr concentration, and that any Pr^{4+} that may be present resides on the Y site. Both of these results are in contrast to the results of Lytle *et al.*

Our result is in striking agreement with the $4+/$ hybridization model put forth by Fehrenbacher and Rice,¹⁸ which predicts that the Pr^{3+} state will exist 60–70% of the time. A ligand hole localized on the Pr-O(2)/O(3) bond would remove a hole from the conduction band and yield a formal Pr^{4+} site. The resulting Pr^{4+} -O bond length would likely be significantly shorter than the Pr^{3+} -O bond, based on the observed bond lengths in other materials. Although we cannot give a precise estimate of the number of short bonds present, our results are consistent with their prediction.

C. The question of the relative position of O(4)

The Cu *K*-edge data for PBCO are consistent with the diffraction results of Lowe-Ma and Vanderah²¹ which show the axial oxygen [O(4)] to be pushed toward the planar Cu site when compared to the YBCO structure (Table IV). The comparison to YBCO is properly made by taking the differences in the lattice parameters *a*, *b*, and *c* into account. Therefore, we also show the bond lengths for “pseudo-YBCO” which is calculated using the lattice parameters for PBCO from Lowe-Ma and Vanderah²¹ and the relative atomic positions of YBCO from Beno *et al.*³¹ The difference in the Cu(2)-O(4) distance between the diffraction and the XAFS results can be explained by comparing the Cu(2)-O(4) distance as a function of oxygen concentration for *R*1:2:3-type materials. In all these materials that have been measured, the Cu(2)-O(4) distance decreases with increasing oxygen concentration. Our result is consistent with this trend (see Ref. 21). An extrapolation of the measured Cu(2)-O(4) distance as a function of oxygen concentration in PBCO,²¹ to an O content of 6.98, yields a bond length of 2.23 Å, in excellent agreement with our result of 2.22 Å.

D. The question of clustering in *RBCO:Pr* (*R*=rare earth and Y)

An interesting property of $R_{1-x}\text{Pr}_x\text{Ba}_2\text{Cu}_3\text{O}_7$ is that the larger the rare-earth radius, the lower the Pr concentration required to completely suppress T_c . It has been suggested²⁵ that this is evidence for clustering of Pr in YBCO:Pr (where the ionic-size difference is comparatively large), thereby maximizing the superconducting Y-Y pairs of cells within a crystal. We had expected that both the Pr and Y *K*-edge data would be very sensitive to this clustering, by giving the number of neighboring Y and Pr atoms. The data in Figs. 4 and 5 show a significant change in the structure near 3.5 Å where the Y or Pr neighbor peak occurs, compared to the pure materi-

als YBCO and PBCO. This means that in the 30% and 50% samples there are both Y and Pr neighbors at each Y-Pr site. If large scale clustering were present, these significant changes in the XAFS would not occur. Unfortunately, fits that try to precisely determine the ratio of Pr to Y neighbors are plagued by interference effects from the Y-Ba and Y-Y peaks, as described in Sec. IV C, which reduces our sensitivity. Consequently, we cannot differentiate between a random distribution and small clusters.

VI. CONCLUSION

In summary, we have collected XAFS data on samples with several different concentrations of Pr in $\text{Y}_{1-x}\text{Pr}_x\text{Ba}_2\text{Cu}_3\text{O}_7$ and on CeO_2 at the Y, Pr, Cu, and Ce *K* edges. The main result of this investigation is that the XAFS data and analysis show that disorder in the oxygen environment around the praseodymium clearly exists. This disorder is most obvious when comparing the first oxygen peak in CeO_2 to the first oxygen peak in $\text{PrBa}_2\text{Cu}_3\text{O}_7$, which shows a 60% reduction in the Pr-O peak. The amplitude of this peak clearly shrinks with increasing Pr concentration.

This PBCO data is best fit by two harmonic radial distributions for the Pr-O bond, which are centered at $2.27_{-0.12}^{+0.03}$ Å and 2.45 ± 0.01 Å in PBCO. The shorter bond may be broader than the longer one by as much as a factor of 3. The magnitude of this distortion agrees well with the change in bond length in other Pr oxides between Pr^{4+} -O (2.18–2.32 Å) and Pr^{3+} -O (2.33–2.66 Å) and is therefore the first structural evidence of a split in the Pr-O bond lengths, and strong evidence for a mixed valent state of Pr in $\text{Y}_{1-x}\text{Pr}_x\text{Ba}_2\text{Cu}_3\text{O}_7$.

We have also verified some results of previous measurements. By comparing the Pr *K*-edge data to FEFF5 simulations of $\text{PrBa}_2\text{Cu}_3\text{O}_7$ with Pr at the Y site and at the Ba or Cu(2) site, we see very little evidence for any of the Pr existing on the Ba or the Cu(2) site (upper limits of 8% and 10%, respectively). In addition, Cu *K*-edge data indicate the O(4) site has moved closer to the Cu(2) site (in agreement with Ref. 21) and therefore may impede charge transfer between the planes and the chains.

ACKNOWLEDGMENTS

We especially wish to thank G. G. Li, J. Rehr, and T.H. Geballe for several useful discussions. The experiments were performed under University PRT beamtime at the Stanford Synchrotron Radiation Laboratory, which is operated by the U.S. Department of Energy, Division of Chemical Sciences, and by the NIH, Biomedical Resource Technology Program, Division of Research Resources. The work is supported in part by NSF Grant No. DMR-92-05204.

- ¹ (a) P.H. Hor, R.L. Meng, Y.Q. Wang, L.Gao, Z.J. Huang, J. Bechtold, K. Forster, and C. W. Chu, *Phys. Rev. Lett.* **58**, 1891 (1987); (b) S. E. Brown, J. D. Thompson, J. O. Willis, R. M, Aiken, E. Zirgniebl, J. L. Smith, Z. Fisk, and R. B. Schwarz, *Phys. Rev. B* **36**, 2298 (1987).
- ² L.F. Schneemeyer, J. V. Wasczak, S. M. Zahurak, R. B. Van Dover, and T. Siegrist, *Mater. Res. Bull.* **22**, 1467 (1987).
- ³ D. W. Murphy, S. Sunshine, R. B. Van Dover, R. J. Cava, B. Batlogg, S. M. Zahurak, and L. F. Schneemeyer, *Phys. Rev. Lett.* **58**, 1888 (1987).
- ⁴ L. Soderholm, K. Zhang, D. G. Hinks, M. A. Beno, J. D. Jorgensen, C. U. Segre, and Ivan K. Schuller, *Nature (London)* **328**, 604 (1987).
- ⁵ J. B. Boyce, F. Bridges, T. Claeson, R. S. Howland, and T. H. Geballe, *Phys. Rev. B* **36**, 5251 (1987).
- ⁶ (a) Y. Dalichaouch, M. S. Torikachvili, E. A. Early, B. W. Lee, C. L. Seaman, K. N. Yang, H. Zhou, and M. B. Maple, *Solid State Commun.* **65**, 1001 (1988); (b) A. Kebede, C. S. Jee, J. Schwegler, J. E. Crow, T. Mihalisin, G. H. Myer, R. E. Salomon, P. Schottmann, M. V. Kuric, S. H. Bloom, and R. P. Guertin, *Phys. Rev. B* **40**, 4453 (1989).
- ⁷ M. Bickel, G. L. Goodman, L. Soderholm, and B. Kanelakopoulos, *J. Solid State Chem.* **76**, 178 (1988).
- ⁸ L. Soderholm, C.-K. Loong, G.L Goodman, and B.D. Dabrowski, *Phys. Rev. B* **43**, 7923 (1991).
- ⁹ H.-D. Jostarndt, U. Walter, J. Harnischmacher, J. Kalenborn, A. Severing, and E. Holland-Moritz, *Phys. Rev. B* **46**, 14872 (1992).
- ¹⁰ E. E. Alp, G. K. Shenoy, L. Soderholm, G. L. Goodman, D. G. Hinks, and B. W. Veal, in *High-Temperature Superconductors*, edited by M. B. Brodsky, R. C. Dynes, K. Kitazawa, and H. L. Tuller, *MRS Symposia Proceedings No. 99* (Materials Research Society, Pittsburgh, 1988), p. 177.
- ¹¹ S. Horn, J. Cai, S. A. Shaheen, Y. Jeon, M. Croft, C. L. Chang, and M. L. denBoer, *Phys. Rev. B* **36**, 3895 (1987).
- ¹² F. W. Lytle, G. van der Laan, R. B. Greeger, E. M. Larson, C. E. Violet, and J. Wong, *Phys. Rev. B* **41**, 8955 (1990).
- ¹³ N. Neukirch, C. T. Simmons, P. Sladeczek, C. Laubschat, O. Strebel, G. Kaindl, and D. D. Sarma, *Europhys. Lett.* **5**, 567 (1988).
- ¹⁴ J. Fink, N. Ncker, H. Romberg, M. Alexander, M. B. Maple, J. J. Neumeier, and J. W. Allen, *Phys. Rev. B* **42**, 4823 (1990).
- ¹⁵ Y. X. Jia, J. Z. Liu, A. Matsushita, M. D. Lan, P. Klavins, and R. N. Shelton, *Phys. Rev. B* **46**, 11745 (1992).
- ¹⁶ J.-S. Kang, J. W. Allen, B.-W. Lee, M. B. Maple, Z.-X. Shen, J. J. Yeh, W. P. Ellis, W. E. Spice, and I Lindau, in *High Temperature Superconductivity, Electronic Structure*, edited by A. Bianconi and A. Marcelli (Pergamon, Oxford, 1989), p. 225.
- ¹⁷ G. Cao, J. W. O'Reilly, J. E. Crow, J. Boliva, D. Nichols, and S. T. Ting, *Bull. Am. Phys. Soc.* **38**, 782 (1993).
- ¹⁸ R. Fehrenbacher and T. M. Rice, *Phys. Rev. Lett.* **70**, 3471 (1993).
- ¹⁹ M. E. López-Morales, D. Ríos-Jara, J. Tagüeña, R. Escudero, S. La Placa, A. Bezinge, V. Y. Lee, E. M. Engler, and P. M. Grant, *Phys. Rev. B* **41**, 6655 (1990).
- ²⁰ J. J. Neumeier, T. Bjørnholm, M. B. Maple, J. J. Rhyne, and J. A. Gotas, *Physica C* **166**, 191 (1990).
- ²¹ C. K. Lowe-Ma and T.A. Vanderah, *Physica C* **201**, 233 (1992).
- ²² M. Guillaume, P. Allenspech, J. Mesot, B. Roessli, U. Staub, P. Fischer, and A. Furrer, *Z. Phys. B* **90**, 13 (1993).
- ²³ R. W. G. Wyckoff, *Crystal Structures* (John Wiley & Sons, New York, 1963).
- ²⁴ C. H. Booth, F. Bridges, P. Cervantes, J. Boyce, and T. Claeson, in *Applications of Synchrotron Radiation Techniques to Materials Science*, edited by D. L. Perry, N. D. Shinn, R. L. Stockbauer, K. L. D'Amico, and L. J. Terminello, *MRS Symposia Proceedings No. 307* (Materials Research Society, Pittsburgh, 1993), p. 117.
- ²⁵ W. J. Zhu, P. Liu, and Z. X. Zhao, *Physica C* **199**, 285 (1992).
- ²⁶ T. M. Hayes and J. B. Boyce, in *Solid State Physics*, edited by H. Ehrenreich, F. Seitz, and D. Turnbull (Academic, New York, 1982), Vol. 37, p. 173.
- ²⁷ J. Mustre de Leon, J.J. Rehr, and S. I. Zabinsky, *Phys. Rev. B* **44**, 4146 (1991).
- ²⁸ B. W. Holland, J. B. Pendry, R. F. Pettifer, and J. Bordas, *J. Phys. C* **11**, 633 (1978).
- ²⁹ G. G. Li, F. Bridges, and G.S. Brown, *Phys. Rev. Lett.* **68**, 1609 (1992).
- ³⁰ S.-L. Lin, E. A. Stern, A. J. Kalb (Gilboa), and Y. Zhang, *Biochemistry* **30**, 2323 (1991).
- ³¹ M.A. Beno, L. Soderholm, D.W. Capone II, D.G. Hinks, J. D. Jorgensen, J. D. Grace, I. K. Schuller, C. U. Segre, and K. Zhang, *Appl. Phys. Lett.* **51**, 57 (1987).